IOP PUBLISHING PHYSICS IN MEDICINE AND BIOLOGY

Phys. Med. Biol. **53** (2008) 4651–4665 doi:10.1088/0031-9155/53/17/013

A scintillating gas detector for 2D dose measurements in clinical carbon beams

E Seravalli[1,5], M de Boer[1], F Geurink[2], J Huizenga[2], R Kreuger[2], J M Schippers[3], C W E van Eijk[2] and B Voss[4]

[1] Foundation for Fundamental Research and Matter (FOM), Utrecht, The Netherlands
[2] Faculty of Applied Sciences, Delft University of Technology, Delft, The Netherlands
[3] Paul Scherrer Institute, Villigen, Switzerland
[4] GSI Gesellschaft für Schwerionenforschung mbH, Darmstadt, Germany

E-mail: e.seravalli@tudelft.nl

Received 2 June 2008, in final form 13 July 2008
Published 11 August 2008
Online at stacks.iop.org/PMB/53/4651

Abstract

A two-dimensional position sensitive dosimetry system based on a scintillating gas detector has been developed for pre-treatment verification of dose distributions in hadron therapy. The dosimetry system consists of a chamber filled with an Ar/CF_4 scintillating gas mixture, inside which two cascaded gas electron multipliers (GEMs) are mounted. A GEM is a thin kapton foil with copper cladding structured with a regular pattern of sub-mm holes. The primary electrons, created in the detector's sensitive volume by the incoming beam, drift in an electric field towards the GEMs and undergo gas multiplication in the GEM holes. During this process, photons are emitted by the excited Ar/CF_4 gas molecules and detected by a mirror-lens-CCD camera system. Since the amount of emitted light is proportional to the dose deposited in the sensitive volume of the detector by the incoming beam, the intensity distribution of the measured light spot is proportional to the 2D hadron dose distribution. For a measurement of a 3D dose distribution, the scintillating gas detector is mounted at the beam exit side of a water-bellows phantom, whose thickness can be varied in steps. In this work, the energy dependence of the output signal of the scintillating gas detector has been verified in a 250 MeV/u clinical ^{12}C ion beam by means of a depth–dose curve measurement. The underestimation of the measured signal at the Bragg peak depth is only 9% with respect to an air-filled ionization chamber. This is much smaller than the underestimation found for a scintillating Gd_2O_2S:Tb ('Lanex') screen under the same measurement conditions (43%). Consequently, the scintillating gas detector is a promising device for verifying dose distributions in high LET beams, for example to check hadron therapy treatment plans which comprise beams with different energies.

[5] Address for correspondence: Department of Radiation, Radio nuclides and Reactors, Division RD&M, Delft University of Technology, Mekelweg 15, 2629 JB Delft, The Netherlands.

1. Introduction

The introduction of dynamic intensity modulation in hadron radiotherapy requires additional and efficient methods for pre-treatment dose verification. Online measurements of beam parameters, such as intensity and profile, do not suffice for the quality control of this advanced treatment technique. It is important to perform simultaneous dose measurements at many different points in the irradiation volume because the dose may be correct at some points in the field while it can be wrong at other points. Especially spatial dose gradients are of particular concern.

3D dose measurements with a standard ionization chamber are time consuming because they require a complete application of the treatment field for each single measurement. In order to overcome this limitation, several methods are being developed to measure the dose in three or two dimensions at once. MRI gel dosimetry (Ramm *et al* 2000, Maryansky *et al* 1993, Olsson *et al* 1990) provides 3D dose information but it has the disadvantage that a magnetic resonance imaging unit is needed for evaluation. 3D arrays of ionization chambers (Karger *et al* 1999) present reliable dosimetric properties, but do not have satisfactory spatial resolution (∼5–6 mm). Stacks of ionization chambers with strip-segmented cathodes for 2D readout have a better spatial response in a plane perpendicular to the beam, but they do not provide full 2D dose information in that plane (only two projections of the beam profile in that plane) (Bonazzola *et al* 1998, Brusasco *et al* 2000). The use of stacks of films (Lomax *et al* 2001) gives dose information with very high spatial resolution, but the film measurement evaluation is time consuming. Scintillating screens (Boon *et al* 1998, Safai *et al* 2004) coupled to a CCD camera allow online measurements of dose distributions with a 2D spatial resolution nearly as good as the film in a plane perpendicular to the beam. However, their response suffers from saturation. The saturation is due to the combination of three effects: a quenching of the light production process due to the ionization density of the particle tracks, the non-tissue equivalence of the scintillator material and the non-infinitesimal thickness of the detection volume (Boon *et al* 1998).

A patient treatment plan is usually composed of a series of hadron beams having different energies. This gives additional complications as, for high LET (linear energy transfer) radiation, the response of gels, films and scintillating screens depends on the energy. The response of these detectors decreases for low particle energies due to saturation. As a consequence, positioned at the end of the depth–dose curve, the Bragg peak depth, these detectors underestimate the dose with respect to the beginning, the plateau, of the curve. A correction for this energy dependence is difficult to apply because the composition of the beam energies in the treatment plan at each position in the irradiated volume as well as the corresponding detector responses must be known.

We have developed a dosimetry system based on a scintillating gas detector coupled to a CCD camera for pre-treatment verification of dose distributions in hadron beams. The dosimetry system consists of a chamber filled with an Ar/CF_4 scintillating gas mixture, inside which two cascaded gas electron multipliers (GEMs) (Sauli 1997) are mounted. A GEM is a thin kapton foil with copper cladding and a regular pattern of sub-mm holes. The primary electrons, created in the sensitive volume of the detector by the incoming beam, drift in an electric field towards the GEMs and undergo gas multiplication in the GEM holes. During this process, photons are emitted by the excited Ar/CF_4 gas molecules and detected by a mirror-lens-CCD camera system. The intensity distribution of the measured light spot is proportional to the two-dimensional hadron dose distribution deposited in the detector sensitive volume. The system is a follow-up of the scintillating Gd_2O_2S:Tb ('Lanex') screen setup (Boon *et al* 1998, 2000).

With gas as a primary detection medium, we expect a smaller energy dependence of the detector response for high LET radiation beams if compared to the signal of a scintillating screen. First, the light production process in a scintillating gas detector does not suffer from the quenching of the scintillation process due to the ionization density of the particle tracks present in the Lanex screen. In fact, in the scintillating gas detector, the photons are emitted by electron-excited gas molecules during the gas multiplication process. Secondly, the employed Ar/CF_4 scintillating gas mixture has a better tissue equivalence and a lower mass density than the scintillating screen (Seravalli *et al* 2007). We expect a 2D spatial resolution in the sub-mm level because of the low Ar/CF_4 diffusion coefficient. Moreover, the combination of the high degree of granularity of the GEM holes and of the CCD camera allows imaging with high resolution. Furthermore, a faster and brighter response than obtained with a Lanex screen is anticipated.

The energy dependence of the scintillating gas detector has already been verified in a proton- (Fetal *et al* 2003) and alpha-particle beam (Seravalli *et al* 2007). In the latter case, the underestimation of the measured signal at the Bragg peak depth was only a few percent with respect to that of an air filled ionization chamber and much smaller than the one presented by a scintillating Lanex screen. The small signal underestimation was attributed to the ionization density in the alpha particle tracks (Seravalli *et al* 2007).

In the present work, we report on the first results of the scintillating gas detector operated in a clinical ^{12}C ion beam and we compare its response along a depth–dose curve to that of an air-filled ionization chamber and to that of a scintillating Lanex screen.

2. Methods and materials

2.1. Detector setup

The detector, represented in figure 1, consists of a $350 \times 350 \times 50$ mm^3 aluminium chamber continuously flushed (9 l h^{-1}) with an Ar/CF_4 92/08 volume percentage gas mixture at 1 atm. Inside the chamber, two cascaded GEMs, produced at CERN (Sauli 1997) and named GEM_1 and GEM_2, have been mounted.

The 100×100 mm^2 GEMs with 60 μm diameter double conical holes at a pitch of 90 μm are glued onto aluminium frames. 25 μm thick aluminized Mylar foils are used as an entrance window and cathode. The entrance window has an opening of 150×150 mm^2. The gap between the cathode and GEM_1 (*drift gap*) is 3.2 mm, while the gap between the two GEMs (*transfer gap*) is 4.2 mm. The 170×170 mm^2 exit window located 35 mm behind GEM_2 is made of 3 mm thick Duran 50 glass. The gap between GEM_2 and the exit window is named *light gap*.

The photons produced in the electron avalanches are detected by means of a low dark-current Apogee 1E camera coupled to a Tamron 171A zoom lens. The camera is equipped with a Kodak KAF-0401E CCD with a quantum efficiency of about 62% at ~640 nm that matches the emission spectrum of the Ar/CF_4 gas mixture (Fraga *et al* 2003). The camera is placed outside the beam to ensure low background radiation onto it. A mirror tilted by 45° reflects the photons towards the camera. The distance between the detector exit window and the mirror is chosen so as to avoid reflections from the mirror back to the window. The light path is enclosed in a light-tight plastic tube that shields it from other light sources in the treatment room. The CCD camera is focused on GEM_2 by means of a 100 mm diameter transparent foil with a 10 mm pitch grid, temporarily mounted at the GEM_2 location. The optical magnification factor of the whole setup is 0.043, leading to 1 pixel (9 μm $\times$ 9 μm) on the CCD being equivalent to 207 μm $\times$ 207 μm at the position of GEM_2. The CCD signal

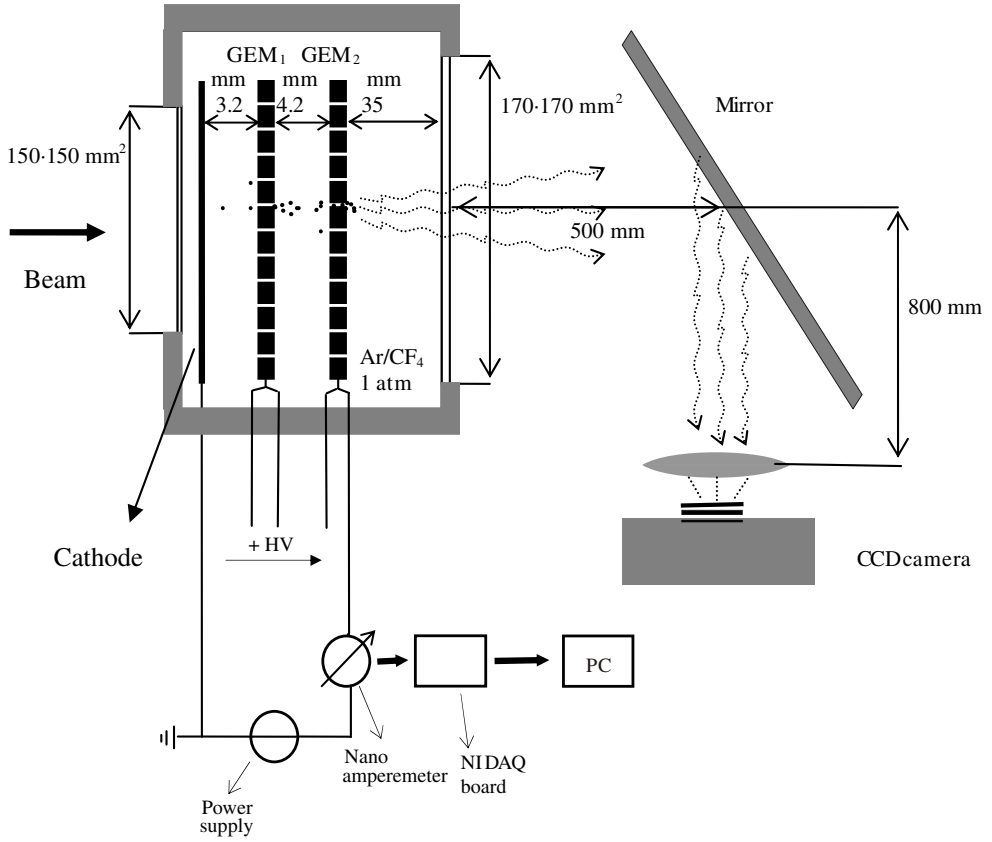

Figure 1. Schematic representation of the scintillating GEM detector setup. The beam enters from the left side. For visualization purposes, only the nano-amperemeter of the last surface of GEM_2 is shown.

per pixel is expressed in analogue-to-digital units (ADU), 1 ADU being equivalent to 8.4 electrons' collected charge on the CCD camera. During the measurements, the CCD camera is cooled down to -20 °C.

Simultaneously to the light signal, the cathode and GEMs currents are measured for a better understanding of the detector operation. The cathode is grounded while each GEM surface is connected to an individual channel of a positive CAEN HV power supply (SY127/A231) with positive polarity. Nano-amperemeters, built in our electronics workshop, measure the currents flowing to the cathode and the GEM surfaces. These meters are connected in series with the supply line of each HV channel. The nano-amperemeter monitoring the current flowing to the cathode has 10 MΩ impedance; the ones measuring the currents flowing to the surfaces of GEM_1 and GEM_2 have 200 kΩ and 56 kΩ impedances, respectively, which yields to a precision of a few tens of nA on the current measurement. These impedance values were chosen to have a well-detectable signal and at the same time a negligible voltage drop across them (<0.5 V) for the expected beam flux. A PC-controlled National Instruments DAQ board samples the measured currents every 1 ms.

All experiments have been performed with voltages across the GEMs, ΔV_{GEM1} and ΔV_{GEM2}, set respectively to 350 V and 340 V, as well as with drift (E_{d}) and transfer (E_{t}) fields

of respectively 1 kV cm^{-1} and 1.5 kV cm^{-1}. These working conditions guaranteed stable detector operation for the applied beam rate.

The temperature and pressure inside the detector were monitored by means of a sensor mounted on the detector chamber.

2.2. The light signal

The light signal S recorded per carbon ion on the CCD camera is proportional to the Ar/CF_4 photon yield, Y. According to the literature (Fraga *et al* 2002), the latter is expressed in number of photons per secondary electron. *Secondary electron* indicates, in this case, the total number of electrons, after gas multiplication by the two cascaded GEMs, which is collected on the GEM_2 surface facing the exit window. In other words, it is the product of the number of primary electrons created per carbon ion in the *drift gap* ($n_e \sim 2092$ at the *plateau*) and the detector gas gain, G. The relationship between S and the Ar/CF_4 photon yield can be described as

$$S = f \cdot Y \cdot G \cdot n_e \text{ (ADU/carbon ion)} \tag{1}$$

where f is the proportionality factor given by the product of the inverse of the CCD camera gain, 0.12 ADU/e$^-$, and the probability that a photon reaches the CCD camera and interacts with its pixels creating an electron. This probability, $\sim 2.7 \times 10^{-6}$, takes into account the CCD camera quantum efficiency, the transmission of the optical elements and the optical solid angle.

Given the spread of Ar/CF_4 photon yield values reported in the literature (Fetal *et al* 2003, Fraga *et al* 2003), it is difficult to make an *a priori* estimation of S. Moreover, the gas gain G is not easy to measure because it depends on the Ar/CF_4 ratio, the gas mixture purity, the type of GEMs employed and ambient conditions.

2.3. Irradiation setup

The experiments were performed in the clinical beam line (cave-M) for carbon ion radiotherapy treatment at the synchrotron of GSI, Darmstadt, Germany (Schardt 2007). The irradiation setup is shown in figure 2.

A phantom comprising a water column with remotely controlled variable thickness (0.1 mm precision), sandwiched between two air-filled parallel plate ionization chambers (*Ic-vor* and *Ic-ext* with respect to the beam direction), was positioned at the isocentre of the beam line in order to simulate the depth in tissue. The GEM detector was installed at the beam exit side of the phantom in a plane perpendicular to the beam. It was positioned horizontally and vertically so as to have the beam spot in the detector centre. The signal of the *Ic-ext* was recorded as a reference during each spill using a Keithley charge meter and then summed over the number of spills during a measurement. The scintillating GEM detector was irradiated with a 250 MeV/u ^{12}C beam with a ripple filter of 2 mm thickness of PMMA in the beam path, i.e. a condition used in clinical practice. The insertion of the ripple filter in the beam causes an increase of the beam energy spread as well as a small decrease of the average beam energy, in order to make the sharp carbon ion Bragg peak broader and lower (Weber and Kraft 1999).

The beam was pulsed: the duration (flat-top) of one pulse (spill) was about 2 s with a 50% duty cycle ($\sim$2 s beam on/off). Experiments were performed at a rate of 2×10^6 ions/spill, used in clinical practice.

The detector light and electrical outputs were integrated over 20 spills corresponding to a total dose in water of about 1 Gy. The CCD exposure time of 96 s was set to be slightly longer

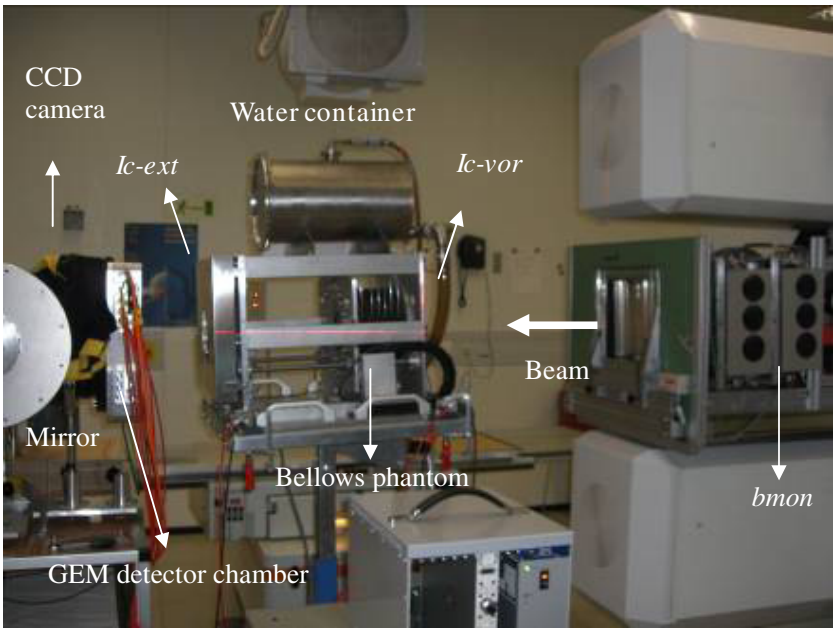

Figure 2. Setup for the irradiation of the scintillating GEM detector in cave-M of Gesellschaft für Schwerionenforschung mbH, Darmstadt, Germany, used for clinical carbon ion radiotherapy treatment. The patient table has been moved to the side and water phantom positioned at the isocentre of the beam line. The scintillating GEM detector is positioned at the beam-exit side of the water phantom.

(This figure is in colour only in the electronic version)

than the beam duration in order to guarantee the complete integration of the emitted light. The dose per spill was calculated multiplying the number of ions per spill by the ion stopping power and dividing by the beam spot area. The FHWM of the beam spot at the minimum water phantom thickness, *plateau*, was about 1 cm and about 2.5 cm at the Bragg peak depth.

The signal of an air-filled ionization chamber (*patient monitor*) positioned in the beam nozzle, was used as a beam monitor, *bmon*. The pulses of the *patient monitor* obtained from a recycling capacitor electronics connected to this ionization chamber were directly recorded by a counter on the PC-controlled National Instruments DAQ board with a sampling time of 1 s.

During the measurements with a standard film and a Lanex scintillating screen, these detectors were placed at the GEM_2 location with respect to the beam. The Bragg curve shown in figures 7 and 8 for the Lanex screen was measured at a different time and with a different camera (van Luijk *et al* 2004) but for identical beam characteristics, as described above.

2.4. Data acquisition and analysis

For a single measurement, the beam is turned on and 20 spills are delivered. As can be seen in figure 3, during this time, *bmon* and the GEM detector currents are sampled on the National Instruments DAQ board.

The emitted light is integrated on the CCD for the exposure time set. The obtained pictures are processed offline using Matlab routines. The dark current of the CCD camera, the light produced in the glass exit window and Ar/CF_4 scintillation in absence of gas multiplication

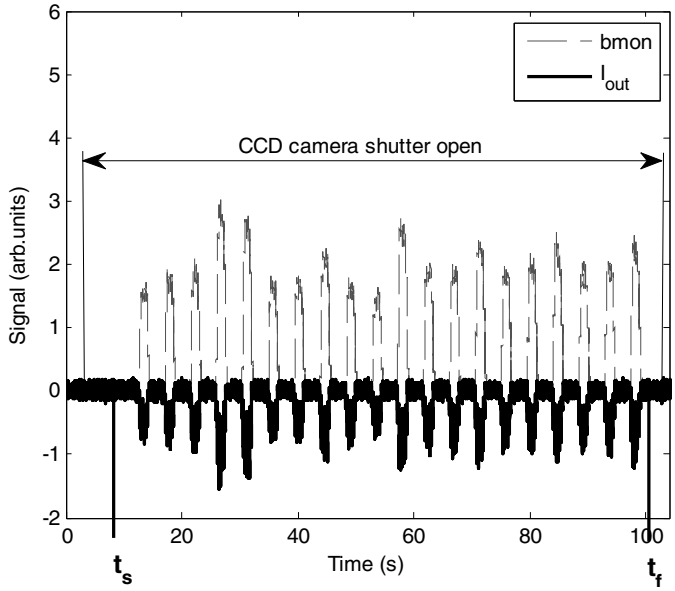

Figure 3. Example of the signals recorded for each single measurement with the scintillating GEM detector. For visualization purposes out of all the electric signals, only I_{out} is represented. CCD camera shutter open is indicated. Dashed line: *bmon* (positive signal); solid line: I_{out} (negative signal). t_s and t_f are the instances in between which q_{out} is evaluated.

are compensated for by subtracting a so-called *background picture*. This *background picture* is taken with the beam on, the camera shutter open for the same exposure period as for a normal picture, and ΔV_{GEM1} and ΔV_{GEM2} set to 0 V while E_d, E_t and the *light gap* electric field set to the standard values.

A 3×3 median filter (Matlab 2007) is applied to the pictures after background subtraction in order to remove large signals on isolated pixels created by the direct interaction of scattered radiation in the CCD. The integrated light yield, L_i, has been calculated by integrating the background corrected picture pixel values in ADU over a circular region of interest. The region of interest is chosen bigger than the beam spot recorded in a picture taken at the Bragg peak depth and it is kept constant for all the pictures.

In figure 4, an example of a picture recorded at the minimum water phantom thickness is shown together with the light-intensity profile along the 1 pixel wide dashed white line. The continuous black line represents the region-of-interest over which the pixel values were integrated.

We define as an output current, I_{out}, the current flowing to the surface of GEM_2 facing the exit window. The I_{out} offset, $\langle I_{offset} \rangle$, is calculated taking the mean value over $N_1 = 2000$ samples of $I_{out}(t_i)$ recorded before the beam starts:

$$\langle I_{offset} \rangle = \frac{\sum_{i=1}^{i=N_1} I_{out}(t_i)}{N_1} \qquad \text{with} \qquad t_{N_1} < t_s. \tag{2}$$

The output charge q_{out} is evaluated summing the offset corrected I_{out} values between t_s (beam starts) and t_f (beam stops) instants, as defined in figure 3. Between t_s and t_f instants, N_2 samples are measured. Δt is the sampling time (1 ms):

$$q_{out} = \left(\sum_{i=s}^{i=f} (I_{out}(t_i) - \langle I_{offset} \rangle) \right) \Delta t \qquad \text{with} \qquad t_s < t_f. \tag{3}$$

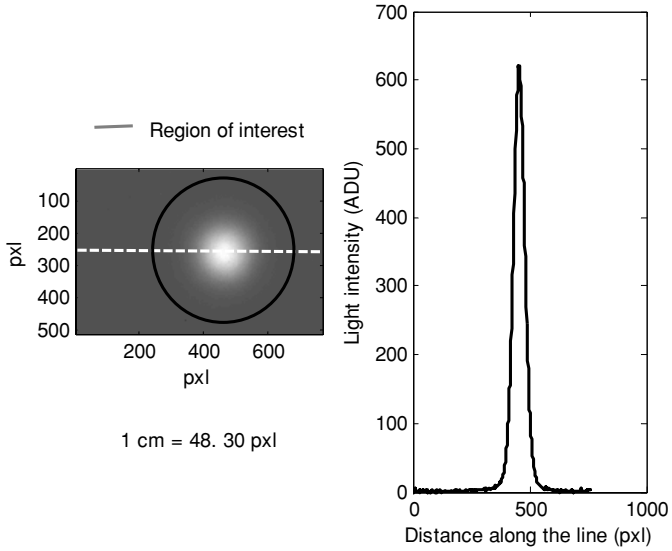

Figure 4. On the left, the example of a picture measured for a carbon ion beam at the minimum water phantom thickness. The continuous black line represents the region of interest over which the pixels are integrated. On the right, the light-intensity profile along the 1 pixel wide dashed white line is shown.

For the measurement of a depth–dose curve, data were taken for increasing water phantom thicknesses, starting at the minimum phantom thickness of 57 mm water equivalent[6] up to the carbon ion range.

In the following, in order to compensate for beam intensity fluctuations, L_i, q_{out} and *Ic-ext* of each measurement are normalized to the *Ic-vor* integrated signal. It has been verified that normalizing L_i, q_{out} and *Ic-ext* to the *bmon* integrated signal leads to the same relative results. For all the detectors used, the *peak-to-plateau ratio* is defined as the ratio of the signal measured at the Bragg peak depth and the one measured at the minimum phantom thickness, *plateau* of the depth–dose curve.

2.5. Uncertainties

The L_i statistical error is calculated taking into account the noise associated with the picture acquisition by means of the CCD camera. The main noise sources are (CCD 2005, Reibel *et al* 2003) as follows.

- The noise associated with the random arrival of photons at any detector. It is the square root of the number of collected photons, since the arrival of photons is governed by Poisson statistics.
- The dark current noise. Although the dark current signal can be corrected for, the noise associated with this signal cannot. The dark current noise is equal to the square root of the dark current signal.

[6] The peak to plateau ratio value depends on the water depth at which the depth–dose curve is normalized to 1. By normalizing the depth–dose curve at 57 mm water equivalent depth instead of 0 mm water depth, an 'error' of about 8% is made on the peak-to-plateau calculation.

- Readout noise, which is the noise produced by the on-chip amplifier and other sources of noise in the data transmission before the signal is converted into a digital representation by the ADC in the CCD.

Typical L_i values measured at the *plateau* and at the Bragg peak depth have an uncertainty of about 0.05% and 0.02%, respectively.

The q_{out} statistical error is evaluated by means of the error propagation formula:

$$\sigma_{q_{out}} = \Delta t \sqrt{N_2 \sigma^2_{I_i(on)} + N_2^2 \sigma^2_{\langle I_{offset} \rangle}} \tag{4}$$

where N_2 is the number of samples between t_s and t_f, $\sigma_{I_i(on)}$ is standard deviation of the sampled values $I_{out}(t_i)$ when the beam is on and $\sigma_{\langle I_{offset} \rangle}$ is the error of $\langle I_{offset} \rangle$. The latter is calculated according to the following equation:

$$\sigma_{\langle I_{offset} \rangle} = \frac{1}{\sqrt{N_1}} \sigma_{I_i(off)} \tag{5}$$

where $\sigma_{I_i(off)}$ is the standard deviation of the samples on which the offset is evaluated by means of equation (2).

A distinction is made between $\sigma_{I_i(off)}$ and $\sigma_{I_i(on)}$ because it was found that the noise in the sampled values is larger when the beam is on, probably due to interference picked up from the accelerator system.

Typical q_{out} values measured at the *plateau* and at the Bragg peak depth have an uncertainty of about 2% and 1%, respectively.

The uncertainty on the *peak-to-plateau ratio* is calculated by means of the error propagation formula, taking into account that the *Ic-vor* integrated signal has a precision of 1.5%, while the *Ic-ext* signal reveals 2.5% (Voss 2007). The *peak-to-plateau ratio* uncertainty is mainly due to the *Ic-vor* precision.

3. Results and discussion

3.1. Scintillating GEM detector response in a pulsed beam

In figure 5, the q_{out} and *Ic-vor* integrated signals are represented as a function of the spill number for a measurement performed at the Bragg peak depth. In this particular case, q_{out} and the integral of the *Ic-vor* signal are calculated for each spill, i.e. every ∼4 s.

q_{out} scales with the *Ic-vor* signal, or in other words, it follows very well the beam intensity fluctuations. The same study could not be performed on L_i values, because the emitted light is integrated over 20 spills. Anyway, L_i is expected to have the same behaviour as q_{out} since, as shown in Seravalli *et al* (2007), it is linearly related to the latter.

3.2. Light intensity and spatial response

At the *plateau*, the scintillating GEM detector light intensity was found to be about three times higher than the Lanex screen signal for identical measurement conditions. Part of this higher signal can be attributed to the fact that the screen response is already affected by saturation at the minimum water phantom thickness in a ^{12}C ion beam (van Luijk *et al* 2004).

In figure 6, the light-intensity profile of a picture taken with the scintillating GEM detector at the *plateau* is compared to the optical density profile of a standard film. The two profiles were taken under the same measurement conditions, and they have been adjusted (without horizontal scaling) in order to make their peaks coinciding. The FWHM of the beam measured by the film is about 10.4 mm assuming a film resolution of about few μm (Aydarous *et al* 2001).

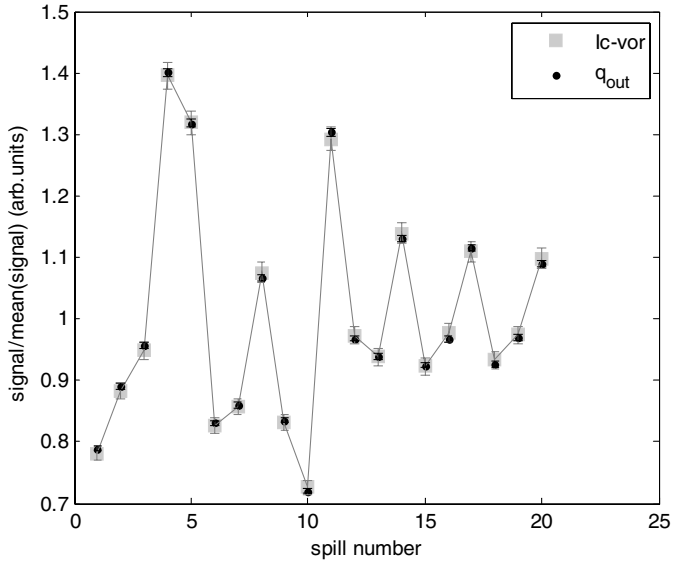

Figure 5. q_{out} and *Ic-vor* calculated for each spill of a measurement at the Bragg peak depth consisting of 20 spills. On the *y*-axis, the ratios of the single data values and the average of all the data values are reported.

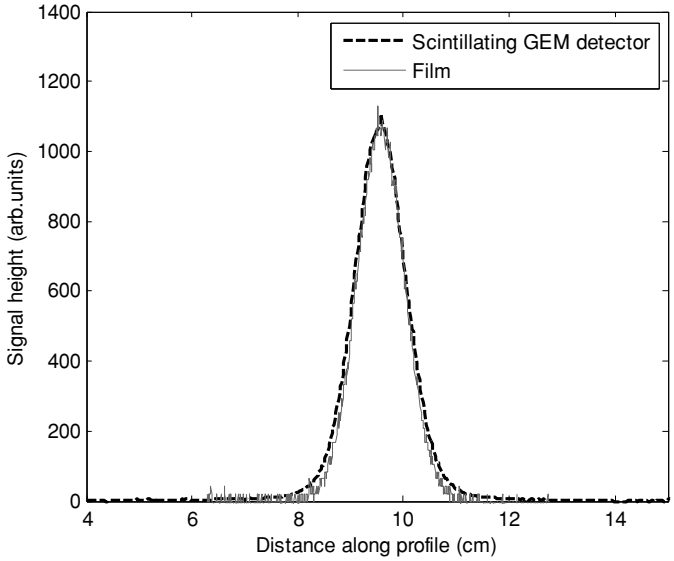

Figure 6. Light-intensity profile of a picture taken with the scintillating GEM detector at the *plateau* compared to the optical density profile of a standard film, measured under identical conditions. For visualization purposes, the profiles have been horizontally shifted and vertically normalized in magnitude in order to make the two peaks coincide.

The FWHM of the scintillating GEM detector profile is found to be 10.9 mm. Consequently, the scintillating GEM detector has a spatial resolution (FWHM) that is $\leqslant$3.3 mm in first approximation.

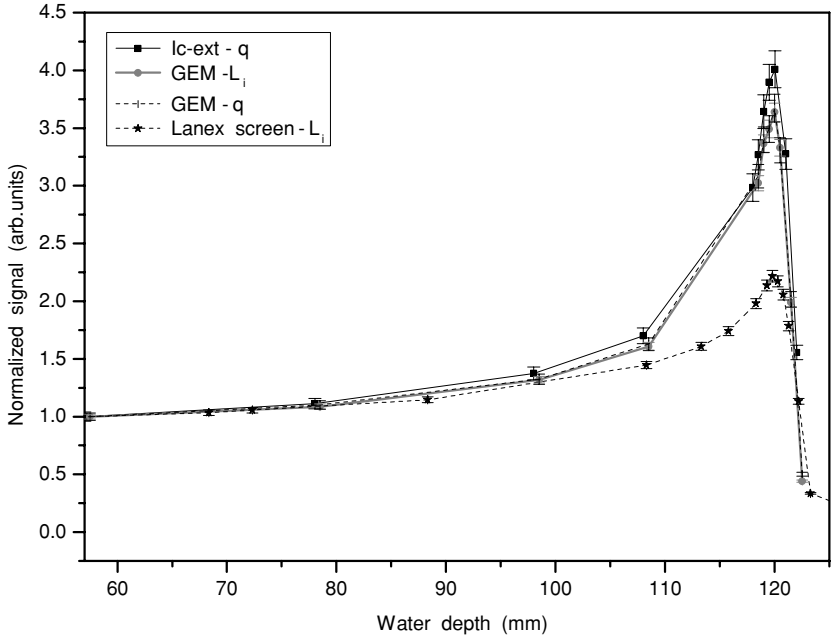

Figure 7. Comparison among Bragg curves measured with the reference ionization chamber, *Ic-ext*, the scintillating GEM detector and the Lanex screen. All curves are normalized to 1 at the minimum water phantom thickness of 57 mm.

Table 1. Peak-to-plateau ratios of the Bragg curves represented in figure 7.

	Peak-to-plateau ratio
Ic-ext–q	4.00 ± 0.16
GEM–L_i	3.64 ± 0.08
GEM–q_{out}	3.67 ± 0.12
Lanex screen–L_i	2.28 ± 0.05

The full width at one-tenth of the maximum (FWTM) is found to be 3 mm wider than that of the film profile. This indicates the presence of tails in the spatial resolution function of the scintillating GEM detector

3.3. Depth–dose curve

In order to study the scintillating GEM detector energy response, we measured a depth–dose curve for an initial energy of the carbon ion beam of 250 MeV/u. In figure 7, the relative L_i and q_{out} Bragg curves are compared to the *Ic-ext* curve measured simultaneously, and to the scintillating screen curve measured at a different moment (van Luijk *et al* 2004) for the same beam conditions.

The curves have been adjusted horizontally in order to have all the Bragg peak positions coinciding, and have been normalized to 1 at the minimum water depth thickness of 57 mm. An expanded view of the Bragg peak region of the curves presented in figure 7 is shown in figure 8. The q_{out} Bragg curve is equal to the L_i curve within the uncertainties, as it was already found in Seravalli *et al* (2007)). As can be seen from table 1, the underestimation of

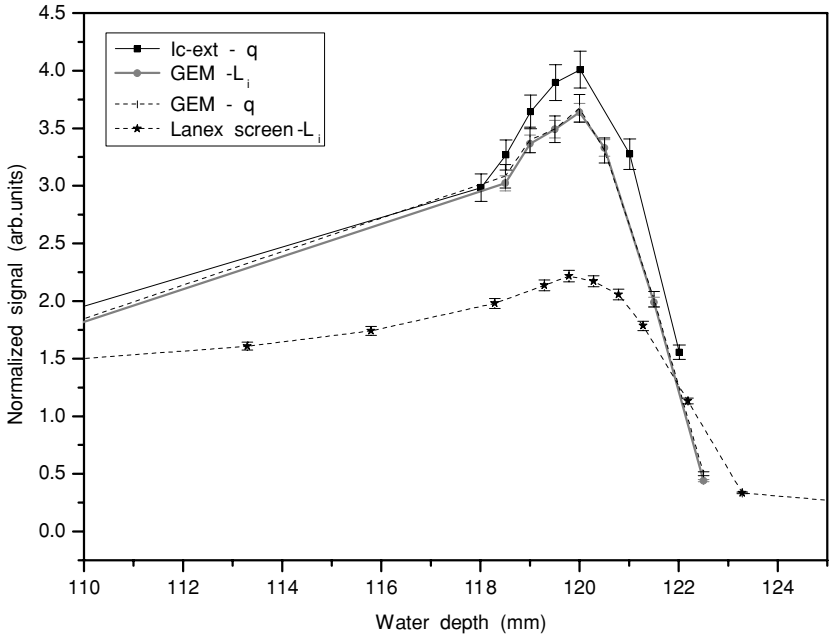

Figure 8. Expanded view of the Bragg peak region for the Bragg curves shown in figure 7.

the signal of the scintillating GEM detector at the Bragg peak depth is about 9% with respect to the *Ic-ext* signal.

This underestimation is much smaller than the one of about 43% measured with the Lanex screen. The same was observed to a lesser extent in an alpha particle beam (Seravalli *et al* 2007). A detailed analysis of the Lanex signal underestimation can be found in Boon *et al* (1998).

Part of the 9% underestimation by the scintillating GEM detector signal can be explained by taking into account the stopping power difference between Ar/CF_4 and air, the filling gas of *Ic-ext*. Measurements in Brusasco *et al* (2000) show that the Bragg peak-to-plateau signal underestimation of an Ar-filled parallel plate ionization chamber is 3.5% with respect to the case when it is filled with air or N_2. These measurements were performed on the same beam line as we did our experiments with a 270 MeV/u beam.

L_i and q_{out} present the same signal underestimation within the uncertainties. Therefore, the cause of the remaining signal underestimation must be related to the charge creation process, which is responsible for both detector signals and/or the recombination in the *drift gap*. However, the latter can be excluded because carbon ion LET recombination effects were not observed for an Ar-filled parallel plate ionization chamber as represented in figure 3 of Kanai *et al* (1998).

When a carbon ion interacts with the gas present in the *drift gap*, clouds of electrons and positive ions are formed around the trajectory of the primary carbon ion. The electron clouds drift towards the GEMs quickly, while the ions move slower in the opposite direction. As can be seen from table 2, the average distance D_{e-} of about 39 mm between the drifting electron clouds created by two different carbon ion tracks in the *drift gap* is quite big compared to the GEM hole pitch dimension of 90 μm.

D_{e-} has been calculated taking into account the carbon ion flux and the electron drift time (0.05 μs in 90/10 Ar/CF_4 (Peisert and Sauli 1984)). If the transversal diffusion coefficient

Table 2. Carbon ion dose rate, flux and average distance D_{e-} between the drifting electron clouds created by different carbon ion tracks in the scintillating GEM detector *drift gap*.

Dose rate (Gy s^{-1})	Carbon ion flux (cm^{-2} s^{-1})	D_{e-} (mm)
0.03	1.3×10^6	39

(roughly 400 $\mu m/\sqrt{cm}$ in 95/05 Ar/CF_4 (Lepeltier 2002)) is also taken into account, one drifting electron cloud extends over about six GEM holes (consequently the radius of one electron cloud is about 0.2 mm). However, it is still quite far from the next drifting electron cloud. Consequently, in one GEM hole there will be electrons created by typically one single primary carbon ion track. So, we suggest that the signal underestimation cannot be attributed to too high a number of electron clouds per GEM hole either. The average distances between ion clouds, calculated taking the diffusion coefficient into account and not reported in table 2, was found to be also larger than the GEM hole pitch. Therefore, space charge effects are not expected to influence the detector output and so to affect the signal at the Bragg peak depth.

On the other hand, a 'saturation' of the charge creation process due to too high a number of multiplied electrons per GEM hole cannot be excluded. In fact, the total number of electrons created by a primary carbon ion track and multiplied in the scintillating GEM detector, at the minimum water phantom thickness of the depth–dose curve, is roughly 0.3×10^6 per GEM hole. At the Bragg peak depth, the total number of electrons per hole is about four times higher, $\sim 1 \times 10^6$ electrons. These numbers are quite close to the phenomenological limit for gas multiplication before breakdown (*Raether limit*) (Sauli 1977) that according to the literature for GEM-based detectors is $\sim 10^7$–10^8 electrons per hole (Ivaniouchenkov *et al* 1999)[7]. Therefore, a 'nonlinearity' or 'saturation' of the charge creation process could take place, especially near and at the Bragg peak depth, affecting the detector working conditions. More data are needed to quantify the importance of this effect.

4. Conclusions

We have developed a 2D dosimetry system based on a scintillating gas detector, equipped with two cascaded GEMs in an Ar/CF_4 mixture. The photons emitted by the Ar/CF_4 electron-excited molecules, during the gas multiplication process, are detected by a CCD camera. Simultaneously to the light signal, GEMs currents are also measured for a better understanding of the detector operation. In this paper, we presented the first investigation of the properties of the scintillating GEM detector irradiated with a ^{12}C ion beam used for clinical radiotherapy treatment.

We have found that the output charge follows very well the beam intensity variations among spills and therefore also the time structure of the pulsed beam. The scintillating GEM detector light intensity at the minimum water depth thickness is three times brighter than the Lanex screen signal. For a typical beam spot, the scintillating GEM detector spatial response (FWHM) is $\leqslant$3.3 mm. However, the scintillating GEM detector has a slightly larger width at one-tenth of the maximum with respect to that of a standard film. This indicates the presence of tails in the spatial resolution function.

The signal of the scintillating GEM detector at the Bragg peak depth is only 9% smaller than that of the reference ionization chamber. This result is much better than the response of the scintillating screen, which is 43% smaller. The small underestimation of the scintillating GEM

[7] The Raether limit depends on the gas mixture, the type of GEMs and the electric field configuration.

detector signal can partly (∼3.5%) be explained by the stopping power difference between Ar/CF_4, filling gas of the GEM detector and air in the reference ionization chamber. Since the charge and light output present the same Bragg peak depth signal underestimation within the uncertainties, the remaining signal underestimation must be related to the charge creation process, which is responsible for creation of both detector outputs. Recombination in the *drift gap* and too high a density of electrons entering a GEM hole in principle may be excluded as causes of signal underestimation. However, a 'saturation' of the charge creation process due to too high a number of multiplied electrons per GEM hole, especially at the Bragg peak depth, cannot be ruled out.

If the expected mm resolution is confirmed, the scintillating GEM detector allows for verification of complex dose distributions in ion beam treatments with their possible steep dose gradients. Verification time will be saved compared to scanning in the water phantom with ionization chambers, or digitizing film measurements. Compared to solid scintillators, corrections for the energy dependence of the response are much smaller or can even be omitted if in the future detector development the signal underestimation at the Bragg peak depth is further reduced. Since we believe that the observed underestimation of the scintillating GEM detector response is mainly due to charge density, it might already be that in proton beams (with lower LET than carbon beams) this detector does not suffer from signal underestimation (<1%). In that case, dose distributions could be quickly verified with mm resolution without knowledge about the beam energy composition.

Further points to be investigated are possible beam rate effects on the detector response and short/long signal reproducibility.

Acknowledgments

The authors would like to thank Dr D Schardt for his support and help while performing the measurements at GSI. This work was supported by the Foundation for Fundamental Research on Matter (FOM).

References

Aydarous A S, Darley P J and Charles M W 2001 A wide dynamic range, high-spatial resolution scanning system for radiochromic dye films *Phys. Med. Biol.* **46** 1379–89

Bonazzola G C, Cirio R, Donetti M, Marchetto F, Mazza G, Peroni C and Zampieri A 1998 Performances of a VLSI wide dynamic range current-to-frequency converter for strip ionization chambers *Nucl. Instrum. Methods* A **405** 111–20

Boon S N, van Luijk P, Böhringer T, Coray A, Lomax A, Pedroni E, Schaffner B and Schippers J M 2000 Performance of a fluorescent screen and CCD camera as a two-dimensional dosimetry system for dynamic treatment techniques *Med. Phys.* **27** 2198–208

Boon S N, van Luijk P, Schippers J M, Meertens H, Denis J M, Vynckier S, Medin J and Grusell E 1998 Fast 2D phantom dosimetry for scanning proton beams *Med. Phys.* **25** 464–75

Brusasco C, Voss B, Schardt D, Krämer M and Kraft G 2000 A dosimetry system for fast measurement of 3D depth–dose profiles in charged-particle tumour therapy with scanning techniques *Nucl. Instrum. Methods* B **168** 578–92

CCD Image Sensor Noise Sources 2005 Application note, www.kodak.com/go/imagers

Fetal S, van Eijk C W E, Fraga F, de Haas J, Kreuger R, van Vuure T L and Schippers J M 2003 Dose imaging in radiotherapy with an $Ar–CF_4$ filled scintillating GEM *Nucl. Instrum. Methods* A **513** 42–46

Fraga F A F, Margato L M S, Fetal S T G, Ferreira Marques R and Policarpo A J P L 2002 Performance of a tracking device based on the GEM scintillation *IEEE Trans. Nucl. Sci.* **49** 281

Fraga M M F R, Fraga F A F, Fetal S T G, Margato L M S, Ferreira Marques R and Policarpo A J P L 2003 The GEM scintillation in $He–CF_4$, $Ar–CF_4$, Ar–TEA and Xe–TEA mixtures *Nucl. Instrum. Methods* A **504** 88–92

Ivaniouchenkov Y, Fonte P, Peskov V and Ramsey B D 1999 Breakdown limit studies in high rate gaseous detectors *Nucl. Instrum. Methods* A **422** 300–4

Kanai T, Sudo M, Matsufuji N and Futami Y 1998 Initial recombination in a parallel-plate ionization chamber exposed to heavy ions *Phys. Med. Biol.* **43** 3549–58

Karger C P, Jäkel O, Hartmann G H and Heeg P 1999 A system for three-dimensional dosimetric verification of treatment plans in intensity-modulated radiotherapy with heavy ions *Med. Phys.* **26** 2125–32

Lepeltier V 2002 www.hep2.fzu.cz/ecfadesy/Talks/Tracking/Lepeltier_Vincent_lepeltier_prague.ppt

Lomax A J *et al* 2001 Intensity modulated proton therapy: a clinical example *Med. Phys.* **28** 317–24

Maryansky M J, Gore J C, Kennan R P and Schulz R J 1993 NMR relaxation enhancement in gels polymerized and cross-linked by ionizing radiation: a new approach to 3D dosimetry by MRI *Magn. Reson. Imaging* **11** 253–8

Matlab *medfilt2* routine, MATLAB®—The Language of Technical Computing, Mathworks Inc., Natick, MA, version 7.0.0.19920(R14) Matlab *medfilt2* routine, MATLAB®—The Language of Technical Computing, Mathworks Inc., Natick, MA, version 7.0.0.19920 (R14) 2007

Olsson L E, Fransson A, Ericsson A and Mattsson S 1990 MR imaging of absorbed dose distribution for radiotherapy using ferrous sulphate gels *Phys. Med. Biol* **35** 1623–31

Peisert A and Sauli F 1984 Drift and diffusion of electrons in gases a compilation *CERN Report* 84-08

Ramm U, Weber U, Bock M, Krämer M, Bankamp A, Damrau M, Thilmann C, Böttcher H D, Schad L R and Kraft G 2000 Three-dimensional BANG™ gel dosimetry in conformal carbon ion radiotherapy *Phys. Med. Biol* **45** N95–102

Reibel Y, Jung M, Bouhifd M, Cunin B and Draman C 2003 CCD or CMOS camera noise characterization *Eur. J. Appl. Phys.* **21** 75

Safai S, Lin S and Pedroni E 2004 Development of an inorganic scintillating mixture for proton beam verification dosimetry *Phys. Med. Biol* **49** 4637–55

Sauli F 1977 Principles of operation of multiwire proportional and drift chambers *CERN Report* 77–09

Sauli F 1997 GEM: a new concept for electron amplification in gas detectors *Nucl. Instrum. Methods* A **386** 531–4

Schardt D 2007 Tumor Therapy with high-energy carbon ion beams *Nucl. Phys.* A **787** 633

Seravalli E, Hendrikse J, Huizenga J, Kreuger R, Schippers J M, Simon A and van Eijk C W E 2007 First Results of a Scintillating GEM Detector for 2D dosimetry in an Alpha Beam *IEEE Trans. Nucl. Sci.* **54** 1271

van Luijk P, Boon S N, Haberer T, Schardt D and Schippers J M 2004 Stopping-power dependence of the light yield in a fluorescent-screen dosimeter *Internal note* Kernfysisch Versneller Instituut, Groningen, the Netherlands

Voss B 2007 Private communication

Weber U and Kraft G 1999 Design and construction of a ripple filter for a smoothed depth dose distribution in conformal particle therapy *Phys. Med. Biol.* **44** 2765–75